ADVANCED MATERIALS

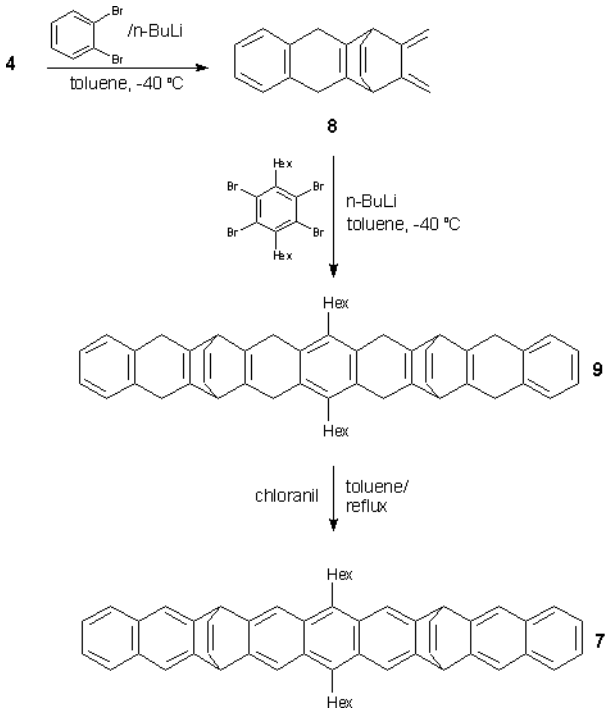

Scheme 3. Scheme showing the synthesis of the nonacene precursor **7**.

temperature. The reaction is quenched with 1 mL of methanol, the solution washed three times with water, and dried over $MgSO_4$. After removing the solvent, chromatography is carried out on the residue on neutral alox. First, unreacted compound **4** and monoadduct **8** are eluted with pentane, and then bis-adduct **5** with petrolether/ethyl acetate. (54 %, m.p.: 191 °C). ^{1}H NMR ($CDCl_3$, ppm) 3.64 (s, 8 H, CH_2), 4.33 (dd, 2 H, CH), 6.99 (dd, 2 H, CH), 7.14 (s, 8 H, aromatic); ^{13}C NMR ($CDCl_3$, ppm) 33.72, 54.79, 126.37, 129.22, 134.8, 139.74, 140.72.

Compound **2**: Compound **5** (0.8 g, 2.64 mmol) and chloranil (1.28 g, 5.28 mmol) are dissolved in toluene (150 mL), and heated for 1.5 h under reflux. After removing the solvent, the residue is purified via chromatography (neutral alox/toluene) (75 %, m.p.: 239 °C). ^{1}H NMR ($CDCl_3$, ppm) 5.33 (dd, 2 H, CH), 7.06 (dd, 2 H, CH), 7.37 (AA′BB′, 4 H, aromatic), 7.71 (AA′BB′, 4 H, aromatic), 7.73(s, 4 H, aromatic); ^{13}C NMR ($CDCl_3$, ppm) 50.74, 121.71, 126, 127.92, 132.25, 138.73, 142.66.

Compound **6a**: A solution of compound **2** (100 mg, 0.32 mmol) and 2,3,4,5-tetrachlorothiophenedioxide (167 mg, 0.64 mmol) in CH_2Cl_2 (4 mL) is heated for 3 days at 70 °C under a pressure of 6 kbar. After the reaction is complete, the solvent is removed under vacuum. Chromatography is carried out on the residue on silica gel with hexane/toluene 4/1 as eluent. The first fraction gives the desired product (75 %). The material can be further purified by recrystallization from dichloroethane/ethyl acetate. ^{1}H NMR (CD_2Cl_2, ppm) 3.54 (s, 2 H, CH), 5.13 (s, 2 H, CH), 7.45 (AA′BB′, 4 H, aromatic), 7.80 (s, 2 H, aromatic), 7.82 (AA′BB′, 4 H, aromatic), 7.86 (s, 2 H, aromatic); ^{13}C NMR (CD_2Cl_2, ppm) 48.08, 48.86, 122.91, 123.93, 124.29, 126.24, 126.35, 128.02, 128.07, 131.38, 132.91, 133.07, 137.47, 139.58.

Compound **6b**: Using the procedure described for the synthesis of compound **6a**, compound **6b** is obtained in a yield of 70 %. ^{1}H NMR (CD_2Cl_2, ppm) 3.58 (s, 2 H, CH), 5.19 (s, 2 H, CH), 7.46 (AA″BB′, 4 H, aromatic), 7.82 (s, 2 H, aromatic), 7.84 (AA′BB′, 4 H, aromatic), 7.86 (s, 2 H, aromatic); ^{13}C NMR (CD_2Cl_2, ppm) 49.74, 51.89, 120.49, 122.87, 123.96, 126.22, 126.33, 128.02, 128.08, 128.72, 132.90, 133.06, 137.51, 139.73.

Received: October 8, 1998
Final version: December 23, 1998

[1] T. Yamabe, K. Tonaka, K. Oheki, *Solid State Commun.* **1982**, *44*, 823.
[2] S. Kivelson, O. L. Chapman, *Phys. Rev. B* **1983**, *28*, 7236.
[3] G. Horowitz, D. Fichou, X. Peng, F. Garnier, *Synth. Met.* **1991**, *41–43*, 1127.
[4] S. F. Nelson, Y. Y. Lin, D. J. Gundlach, T. N. Jackson, *Appl. Phys. Lett.* **1998**, *72*, 1854.
[5] A. Dodabalapur, L. Torsi, H. E. Katz, *Science* **1995**, *268*, 270.
[6] C. J. Drury, C. M. J. Mutsaers, C. M. Hart, M. Matters, D. M. de Leeuw, *Appl. Phys. Lett.* **1998**, *73*, 108.
[7] A. R. Brown, A. Pomp, D. M. de Leeuw, D. B. M. Klaassen, E. E. Havinga, P. Herwig, K. Müllen, *J. Appl. Phys.* **1996**, *79*, 2136.
[8] A. Chollet, M. Wismer, P. Vogel, *Tetrahedron Lett*. **1976**, *47*, 4271.
[9] M. S. Raasch, *J. Org. Chem*. **1980**, *45*, 856.
[10] A. R. Brown, C. P. Jarrett, D. M. de Leeuw, M. Matters, *Synth. Met.* **1997**, *88*, 37.
[11] For an example of the improvement of the characteristics of a pentacene MISFET by priming the substrate, see: Y.-Y. Lin, D. J. Gundlach, S. F. Nelson, T. N. Jackson, *IEEE Electron Device Lett*. **1997**, *18*, 606.

Fabrication and Microstructuring of Hexagonally Ordered Two-Dimensional Nanopore Arrays in Anodic Alumina**

By *An-Ping Li*,* *Frank Müller*, *Albert Birner*, *Kornelius Nielsch*, and *Ulrich Gösele**

The fabrication of nanochannel-array materials has attracted considerable scientific and commercial attention due to their potential utilization in magnetic, electronic, and optoelectronic structures and devices.[1,2] For example, nanoscale patterned arrays have been suggested as recording media to achieve recording densities of more than 100 Gbits/in^2 (~16 Gbits/cm^2), each memory unit being stored in a single array.[3,4] This storage density is much higher than that of current commercial hard disks (3.7 Gbits/in^2, IBM Deskstar 25GP), and also beyond the projected thermal limit of 40 Gbits/in^2 in continuous magnetic films.[5]

Moreover, the application of ordered nanochannel-arrays as two-dimensional photonic crystals has generated increasing interest in recent years.[6–8] When electromagnetic radiation with a wavelength comparable to the periodicity of the array passes through such an array, the dispersion relation is modified according to the array geometry and composition. This is analogous to the effect of a crystalline structure on the behavior of electrons. Hence, the artificially engineered periodic dielectric structures are called photonic crystals.[9] In analogy to semiconductors, certain structures provide a photonic bandgap, an energy region where no photon modes are allowed. Among the applications for these materials are the inhibition or enhancement of spontaneous emission and the fabrication of tunable optical filters and microcavities[10] or waveguides.[9,11]

Anodic porous alumina, which has been studied extensively over the last five decades,[12] has recently been reported to be a typical self-ordered nanochannel material.[13,14] Self-organization during pore growth, leading to a densely packed hexagonal pore structure, has been reported in oxalic, sulfuric, and phosphoric acid solu-

[*] Dr. A. P. Li, Dr. F. Müller, A. Birner, K. Nielsch, Prof. U. Gösele
Max Planck Institute of Microstructure Physics
Weinberg 2, D-06120 Halle (Germany)

[**] The authors thank O. Breitenstein for his help in depositing the aluminum film, and W. Erfurth and Mrs. U. Doß for technical support.

  0935-9648/99/0604-0483 $ 17.50+.50/0

tions.[13–16] The interpore distances of the regularly ordered pore arrangement have been extended to the large range of 50–420 nm.[15] However, the ordered pore arrangements are formed under specific anodizing conditions after a long anodization time, and as a result they can only be observed at the bottom of the films. Masuda and Satoh first demonstrated a two-step fabrication method for straight nanoholes in a thin membrane of porous alumina.[17] The structural characteristics of the ordered porous alumina make it not only a perfect template material for the fabrication of nanoscale structures but also an outstanding candidate material for two-dimensional (2D) photonic crystals, which may show photonic bandgaps that are adjustable in the visible to ultra-violet spectral region. However, in order to realize 2D behavior of ordered nanopore arrays, high aspect ratios (the ratio of the length of a pore to its diameter) would greatly facilitate characterization. In this paper, we report the fabrication of parallel, regularly arranged nanopore arrays with a high aspect ratio in anodic alumina. A lateral microstructuring technique was developed for micromachining bars of porous alumina.

The process of fabricating ordered porous alumina and its microstructuring is outlined in Figure 1. In brief, the ordered nanopore arrays are prepared by using a two-step anodization process. Subsequently, a lithographic technique is applied to microstructure the nanopore arrays.

Detailed descriptions of the first anodization process of aluminum have already been published.[13–16] High purity (99.999 %) aluminum foils were first degreased and then annealed under nitrogen ambient at 400 °C to remove mechanical stresses and to recrystallize the samples. Subsequently, the substrates were electropolished in a mixture of $HClO_4$ and C_2H_5OH to smooth the surface. Anodization was conducted under constant cell potential in three types of aqueous solutions, sulfuric, oxalic, and phosphoric acids, which were used as electrolytes.

Hexagonally ordered pore domains can be prepared by a self-organization process under some specific anodization conditions.[13–16] Because the pores initiate at almost random positions and order thereafter by self-adjusting during a long-time anodization process, pore arrangements on the surface are disordered and have a broad size distribution. Ordered pore domains can only be obtained at the bottom of the layers. Therefore the pores produced in the first anodization step are not parallel to one another. To fabricate ordered nanopore arrays in which the holes are straight and regularly arranged throughout the film, we used a two-step anodization process.

After the first anodization step, the porous alumina was removed by a wet chemical etching in a mixture of phosphoric acid (6 wt.-%) and chromic acid (1.8 wt.-%) at 60 °C. At the bottom of the porous film, there is a thin oxide layer, called the barrier layer, covering the pore bottoms. The barrier layer is not flat but consists of periodically arranged crests and troughs (the topography of the barrier layer can be seen in Fig. 2b). The fluctuation changes the surface of

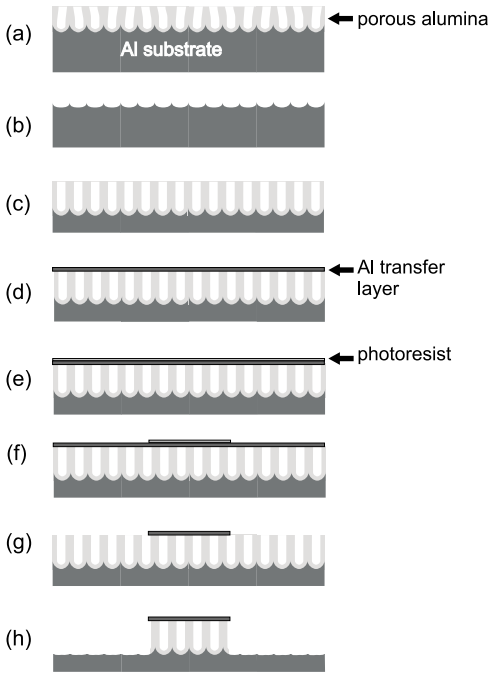

Fig. 1. Schematic diagram of the fabrication and microstructuring processes of a nanopore array in anodic alumina: a) porous alumina obtained in the first anodization, b) etch pits remaining on the aluminum surface after removal of the porous alumina, c) a nanopore array formed in the second anodization, d) evaporation of an aluminum transfer layer, e) coating of photoresist, f) patterning of resist, g) patterning of aluminum layer, h) etching of vertical microstructures.

the aluminum substrate into a dimpled and undulating landscape that has the same spatial ordering as the barrier layer. After the removal of the porous film, the periodic concave patterns that remain, as shown schematically in Figure 1b, act as a self-assembled template for the second anodization process. An ordered nanopore array is obtained after the second anodization if the same parameters are used as in the first anodization step.

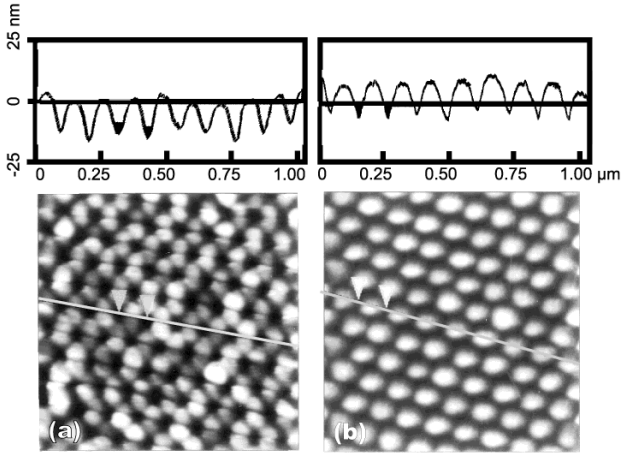

Fig. 2. AFM a) top and b) bottom views of a nanopore array in anodic alumina prepared by two-step anodization. The depth profiles were measured along the lines indicated. The measurements were performed in tapping mode in air and the scan rate was kept at 1 Hz. Anodization was conducted in 0.3 M oxalic acid at 5 °C at 40 V. The remaining aluminum substrate was removed in a saturated $HgCl_2$ solution.

0935-9648/99/0604-0484 $ 17.50+.50/0

ADVANCED MATERIALS

The periodicity of an ordered nanopore array is demonstrated in Figure 2. The two steps of anodization were conducted in 0.3 M oxalic acid under 40 V and at 5 °C. The anodization times of the first and second processes were 20 and 94 h, respectively. Figure 2a shows an atomic force microscopy (AFM) top view image of the nanopore array and a depth profile along a line on the surface. The dark parts correspond to the pores. The period of the pore arrangement or interpore distance is about 112 nm. The roughness of the surface results from the second anodization process and the chemical etching to remove the oxide layer. In order to observe the morphology of the bottom of the nanopore array, the remaining aluminum substrate was removed in a saturated $HgCl_2$ solution. The thickness of the free-standing porous alumina layer was measured under an optical microscope to be about 160 μm. Figure 2b shows an AFM bottom view image exhibiting the morphology of the pore bottoms, where the barrier layer remains. The pore bottoms can be opened with an aqueous phosphoric acid solution. The bright parts correspond to the protruding pore bottoms. The concave–convex topography of the barrier layer can be clearly seen from the depth profile. The period of the pore arrangement is about 115 nm, almost the same as that at the surface of the array. The aspect ratio is about 1400. Such a high aspect ratio is hard to visualize. As examples, Figure 3 shows two cross-sections of the morphology of the pore arrays, where (a) is near the surface and (b) is in the middle. The nanopore arrays are straight and parallel, although there are some defects.

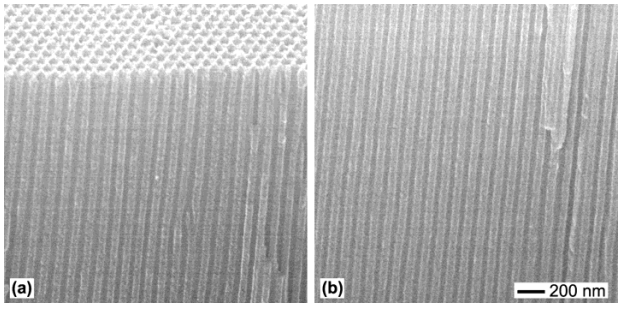

Fig. 3. Scanning electron microscopy images of cross-sectional morphologies of the ordered nanopore arrays: a) near the surface, b) in the middle.

The self-ordering mechanism during the first anodization process of the aluminum was discussed previously.[15,16] It was suggested that the repulsive forces between neighboring pores caused by mechanical stress at the metal/oxide interface promote the formation of hexagonally ordered pore arrangements. The best ordering is achieved for a moderate expansion factor (ratio of the thickness of the alumina layer grown to the aluminum layer consumed) of 1.4, independent of which electrolyte is used. Based on this explanation, we changed anodization parameters while controlling the expansion factor and prepared ordered pore structures with interpore distances of 50, 60, 100, 150, and 420 nm, which corresponds to a pore density range of 6×10^8 to 5×10^{10} cm^{-2} (4–300 Gbits/in^2 storage density if used as a medium for a memory device). Moreover, it was found that ordered domains have sizes in the range 1–5 μm and are separated from neighboring domains with different orientation of the pore lattice by grain boundaries, i.e., the ordered pore arrangements show polycrystalline morphology. The nanopore arrays prepared by using the two-step anodization process have the same structural characteristics as the pore arrangements formed in the first anodization step, since the anodized pore arrays formed in the second step closely resemble their pre-patterns.

For the characterization as a photonic crystal using transmission measurements, the ordered pore arrays have to be structured in a macroscopic way. The structuring processes are shown schematically in Figures 1d–h. An aluminum layer (0.3–1 μm thick, depending on the pore diameters) was first evaporated on the surface to get a medium transfer layer and to improve the flatness, because the surface consists of a regular pattern of holes with walls in between, as shown in Figure 3a. Subsequently, a lithographic process was used to define the microstructure pattern. A positive resist (AR-U4040, Allresist GmbH) was used. A wet chemical etch based on phosphoric and nitric acids with an additional small amount of wetting agent was used to transfer the patterned resist to the Al layer. The Al layer not covered by the resist was completely removed after 30 min of etching. Finally, the porous alumina in the areas of the Al windows was etched down with a chemical etching in an aqueous H_3PO_4 solution (5 wt.-%). Since in the opened area the solution can penetrate into the holes and therefore the etching takes place at the whole oxide/solution interface, the actually removed lateral part is only half of the pore wall thickness, i.e., less than 50 nm in the case of Figure 3. Therefore, the etching is quite fast in the parts with open pores. On the other hand, the Al mask is not attacked by the etching solution, and therefore protects the areas to be obtained as bars afterwards. As a result, a highly selective etch output can be expected although the chemical etch is a microscopically isotropic process under our conditions.

A typical sample obtained by using this lateral microstructuring technique is shown in Figure 4, where the microstructured porous alumina bars are sandwiched by the Al substrate and the Al transfer layer, which can help to limit light in the vertical direction in the case of transmission measurements. If needed, the remaining Al can be removed in a saturated $HgCl_2$ solution as shown in Figure 2. The bars of porous alumina shown in Figure 4a are about 200 μm high and 300 μm wide. The microstructuring technique leads to a sharp edge, which is magnified in Figure 4b. The anisotropy of the whole process can be clearly seen. The side walls of the structures are very steep, and the roughness on the side wall (1–3 μm) is determined by the quality of the mask and the aluminum transfer layer. The undercut between the transfer layer and the porous alumina depends on etching time. If the etching time is too long, an obvious undercut will appear as shown in Figure 5,

  0935-9648/99/0604-0485 $ 17.50+.50/0

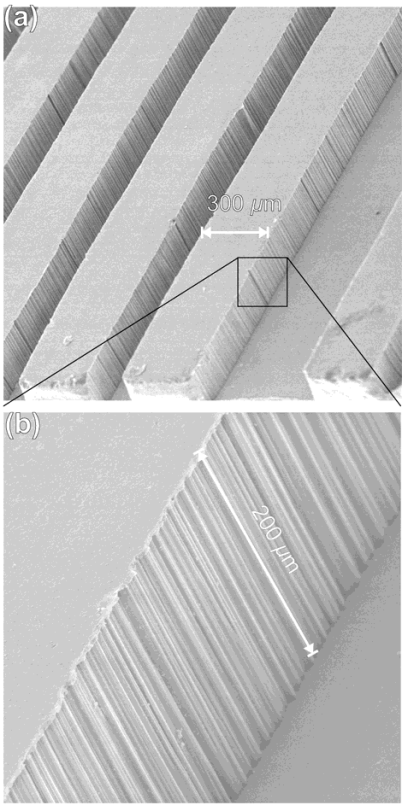

Fig. 4. a) Typical microstructure depth profile. b) An enlarged view of a side wall. The structure height is 200 μm.

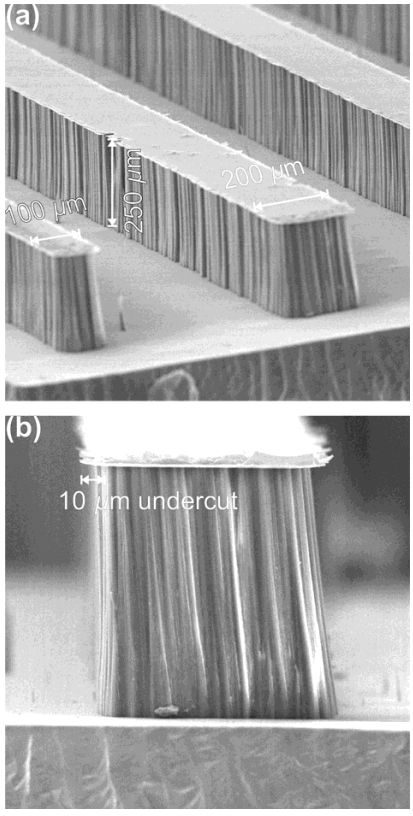

Fig. 5. Depth profile of undercut after inappropriately long chemical etching.

where the bars are about 250 μm high and 100 μm or 200 μm wide and the undercut is up to 10 μm. Moreover, if the etching process is too fast, the solution cannot homogeneously penetrate into the pores and the etching does not take place in the same pore rows as at the top. The side walls of structures then do not correspond to the pore walls of the nanopore arrays. Under these conditions, rough or even sloping side walls will appear as shown in Figure 5b. Overall, using this microstructuring technique, we obtain bars of porous alumina on the aluminum substrate that are 100–400 μm wide, 100–300 μm high, and several millimeters long. The samples had the necessary precision for further applications as photonic crystals. They are well suited for investigations of the optical properties with light traveling perpendicular to the pore axis.

The feasibility of using the ordered porous alumina as a two-dimensional photonic bandgap material has been shown theoretically. Theoretical calculations predict that hexagonally ordered porous alumina shows photonic bandgaps for *H*-polarized light (the magnetic field vector *H* is parallel to the pore axis). The width of the lowest bandgap will depend little on the orientation of light propagation.[18] Although the ordered domains are of polycrystalline distributions, the structures are expected to exhibit interesting photonic crystal properties analogous to the electronic properties of polycrystalline semiconductors. Moreover, the fabrication of photonic monocrystals of porous alumina should also be possible by using an appropriate prepatterning technique. Our group is now working on direct pre-patterning of the aluminum surface by an electron beam lithography technique and fabricating monocrystalline nanopore arrays on aluminum.

In summary, we have fabricated hexagonally ordered nanopore arrays with high aspect ratios based on a self-organization process in anodic alumina. A two-step anodization technique was used to oxidize aluminum in oxalic, sulfuric, and phosphoric acid solutions. The ordered pore arrays are straight and parallel, and of polycrystalline structure. The pore distance can be controlled by changing the anodic electrolyte and the applied voltage. For the characterization as a photonic crystal using transmission measurements, a lithographic microstructuring technique for the ordered nanopore arrays was reported. Bars of porous alumina 100–400 μm wide, 100–300 μm high, and several millimeters long were prepared. The microstructuring technique can also be used to micromachine structures based on porous alumina.

Received: October 26, 1998
Final version: January 13, 1999

[1] R. J. Tonucci, B. L. Justus, A. J. Campillo, C. E. Ford, *Science* **1992**, *258*, 783.
[2] T. W. Whitney, J. S. Jiang, P. C. Searson, C. L. Chien, *Science* **1993**, *261*, 1316.
[3] R. M. White, R. M. H. New, R. F. W. Pease, *IEEE Trans. Magn*. **1996**, *33*, 990.

  0935-9648/99/0604-0486 $ 17.50+.50/0

ADVANCED MATERIALS

[4] D. Routkevitch, A. A. Tager, J. Haruyama, D. Almawlawi, M. Moskovits, J. M. Xu, *IEEE Trans. Electron Dev.* **1996**, *43*, 1646.
[5] P. L. Lu, S. H. Charap, *IEEE Trans. Magn*. **1994**, *30*, 4230.
[6] A. Rosenberg, R. J. Tonucci, H.-B. Lin, E. L. Shirley, *Phys. Rev. B* **1996**, *54*, R5195.
[7] M. D. B. Charlton, S. W. Roberts, G. J. Parker, *Mater. Sci. Eng. B: Solid State Mater. Adv. Technol.* **1997**, *49*, 155.
[8] U. Grüning, V. Lehmann, S. Ottow, K. Busch, *Appl. Phys. Lett*. **1996**, *68*, 747. A. Birner, U. Grüning, S. Ottow, A. Schneider, F. Müller, V. Lehmann, H. Föll, U. Gösele, *Phys. Status Solidi A* **1998**, *165*, 111.
[9] E. Yablonovitch, *Phys. Rev. Lett*. **1987**, *58*, 2059.
[10] J. S. Foresi, P. R. Villeneuve, J. Ferrera, E. R. Thoen, G. Steinmeyer, S. Fan, J. D. Joannopoulos, L. C. Kimerling, H. I. Smith, E. P. Ippen, *Nature* **1997**, *390*, 143.
[11] See, e.g., J. D. Joannopoulos, R. D. Meade, J. N. Winn, *Photonic Crystals: Molding the Flow of Light*, Princeton University Press, Princeton, NJ **1995**.
[12] See, e.g., F. Keller, M. S. Hunter, D. L. Robinson, *J. Electrochem. Soc.* **1953**, *100*, 411. P. Czokan, in *Advances in Corrosion Science and Technology*, Vol. 7 (Ed: M. G. Fontana, R. W. Staehle), Plenum, New York **1980**, p. 239. G. E. Thompson, G. C. Wood, in *Treatise on Materials Science and Technology*, Vol. 23 (Ed: J. C. Scully), Academic, New York **1983**, p. 205.
[13] H. Masuda, K. Fukuda, *Science* **1995**, *268*, 1466.
[14] H. Masuda, F. Hasegawa, S. Ono, *J. Electrochem. Soc.* **1997**, *144*, L127.
[15] A. P. Li, F. Müller, A. Birner, K, Nielsch, U. Gösele, *J. Appl. Phys.* **1998**, *84*, 6023.
[16] O. Jessensky, F. Müller, U. Gösele, *Appl. Phys. Lett.* **1998**, *72*, 1173.
[17] H. Masuda, M. Satoh, *Jpn. J. Appl. Phys.* **1996**, *35*, L126.
[18] R. Hillebrand, private communication.

Synthesis and Mechanistic Studies of Sulfated Meso- and Microporous Zirconias with Chelating Carboxylate Surfactants

By *David M. Antonelli**

Since the discovery of the MS-41 family of molecular sieves[1–5] in the early nineties, a great deal of work has been invested in the synthesis of both mesoporous (pore size > 20 Å) and microporous (pore size < 20 Å) transition metal oxide analogues of these exciting new materials.[6–8] Transition metal oxides have variable oxidation states that can be exploited in the design and synthesis of mesoporous materials with novel catalytic, optical, and magnetic properties not possible with main group oxides. In 1996 the first clear examples of stable transition metal oxide mesoporous molecular sieves appeared.[9] These materials had surface areas of up to 600 $m^2 g^{-1}$ and thermal stabilities, on template removal, of up to 700 °C.[10] Since this initial discovery, examples of mesoporous Zr,[7,11,12] Hf,[8] and Mn[13] oxides have been reported. In 1997 Sun and Ying[14] reported the first example of a microporous transition metal oxide molecular sieve synthesized by liquid-crystal templating. The synthesis of this niobium oxide-based material was accomplished using amines with carbon chains of 4–8 atoms as templating agents. This is a modification of the ligand-assisted templating strategy originally used to synthesize mesoporous niobium oxide.[6c] This has exciting mechanistic implications, as it demonstrates that, because the short-chained surfactants used in the synthesis of these materials do not readily form liquid crystals, micelles may not be involved in the formation of these materials. It also opens the doorway for size-selective transition metal oxides[15] and the fabrication of novel electronic materials.[16] Because zirconia is useful in acid catalysis and in oxygen-sensing devices it is of great importance to synthesize microporous zirconium oxide molecular sieves. Herein is described the synthesis of the first samples of microporous zirconium oxide synthesized through a ligand-assisted templating approach using carboxylate surfactants. This approach can also be modified to yield samples of mesoporous zirconium oxide with significantly higher surface areas than those previously reported for mesoporous zirconia.[7,11,12]

Recent work by Schüth et al. showed that well-defined sulfated and phosphated samples of mesoporous zirconia[7] with high thermal stabilities and surface areas of 280 $m^2 g^{-1}$ could be synthesized with trialkylammonium surfactants and a zirconium oxide precursor. Attempts by our group to extend this approach to microporous materials by using reduced chain lengths led only to the formation of amorphous materials. For this reason, we decided to extend the ligand-assisted templating approach, successful in the synthesis of both meso- and microporous niobia, to the synthesis of microporous zirconia. Surfactants with phosphate head groups were previously established as effective ligand-templating agents in the synthesis of hexagonally packed phosphated titanium oxide mesostructures.[6] Removal of the template by calcination gave materials with surface areas of up to 200 $m^2 g^{-1}$, a narrow pore-size distribution and hexagonally packed, mesoporous regions as shown by transmission electron microscopy (TEM). Later studies on the zirconium analogue of this system[12] demonstrated that retention of phosphate was necessary in maintaining the mesoporosity of the material upon surfactant removal.

Because phosphate surfactants yielded mesostructures of Ti and Zr oxides we chose to investigate other bis- and tris-chelating surfactants which could be more easily removed from the structure without leaving behind unwanted residues such as phosphate. Over the course of our investigations it was found that carboxylate surfactants yielded well-defined hexagonally packed zirconia mesostructures starting from alkoxide precursors at a metal-to-surfactant ratio of 2:1. This approach worked well with surfactant carbon chains from 5 to 18 carbon atoms. In our new procedure the alkoxide was typically combined with the surfactant at room temperature and stirred until a homogeneous solution was obtained. This mixture presumably contained a zirconium–alkoxide carboxylate complex, as the replacement of alkoxides by carboxylates is well-documented. Addition of water resulted in the precipitation of a white solid. The inhomogeneous mixture was then aged in water at pH 5 for

[*] Dr. D. M. Antonelli
Department of Chemistry and Biochemistry
University of Windsor
Windsor, Ontario N9B-3P4 (Canada)

  0935-9648/99/0604-0487 $ 17.50+.50/0